Project Report for Quantum Mechanics II (Spring 2023)

The Casimir Effect

M. Salman Hassan[1] **Anamta Asif**[2]

PHY-312, Department of Physics, SBASSE, LUMS.

E-mail: 25100150@lums.edu.pk, 25100098@lums.edu.pk

Abstract: The Casimir Effect, predicted by Hendrik Casimir in 1948, is an attractive force that emerges when two infinitely large, perfectly conducting, uncharged metallic plates are placed parallel to each other in a vacuum, separated by a few nanometers. This phenomenon can be largely explained through vacuum energies and quantum fluctuations in space and, in recent years, it has been theorized that it might be a manifestation of Van der Waals forces at larger distances. Multiple experiments conducted in the late 1990s confirmed the Effect, paving the way for research in nanotechnology. Our primary objective in this research is to explore the mathematical derivation of the Effect using two regularization techniques and examine the intricacies of experimental setups needed for its verification, especially those by Lamoreaux in 1997 and Mohideen in 1998. Additionally, we briefly address the influence of the type and geometries of the plates used to better understand the potential applications of the Casimir Effect in nanotechnology, more particularly in the Anharmonic Casimir Oscillator (ACO). Toward the end, we discuss some of the practical challenges faced in these applications.

Keywords: Casimir Effect, Casimir Force, Quantum Fluctuations, Nanotechnology, Regularization Techniques, Experiments

Contents

1 Introduction

The existence of quantum fluctuations in the vacuum of the electromagnetic field is a consequence of the Heisenberg Uncertainty Principle:

$$\Delta E \Delta t \geq \frac{\hbar}{2}. \tag{1.1}$$

This principle implies that the zero-point energy of the vacuum cannot be zero; otherwise, this fundamental law of quantum mechanics would be violated. Casimir recognized the implications of this phenomenon and investigated its potential consequences. Although these quantum fluctuations are an inherent aspect of the universe, the vacuum energy itself is in equilibrium throughout space. The zero-point energies are defined by the ground-level energy of the harmonic oscillator, summed over all frequencies in space:

$$E_o = \frac{\hbar}{2} \sum_k |\omega_k|. \tag{1.2}$$

In Casimir's original paper [1], he explored the relationship between the Casimir-Polder effect and Van der Waals forces. The Casimir-Polder effect occurs when two atoms are separated by a distance smaller than the wavelength corresponding to the electron's energy. At this scale, the force between the atoms follows a power law with distance, R^{-7}:

$$F_{vdW} \propto R^{-7}.$$

This equation is valid at the Angstrom level and applies to interactions between two atoms or between an atom and a plate.

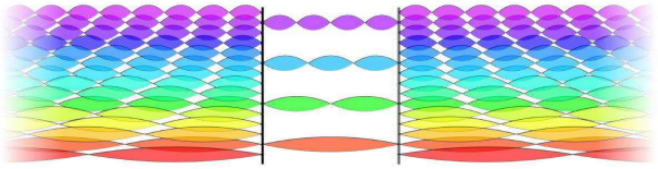

Figure 1: Outside the cavity formed by the plates, all vacuum frequencies are permitted. Inside the cavity, however, vacuum modes have discrete frequencies. Modifying the cavity width alters the mode density compared to free space, resulting in an energy difference.

Casimir wanted to see if these zero-point energies could influence macroscopic objects. Therefore, in 1948 [2], he researched the case of two parallel, infinitely large, uncharged conducting metallic plates placed a few nanometers apart. The number of allowed frequencies between the plates is significantly reduced, and the equilibrium in the region is disturbed. The Dirichlet boundary conditions require a node on the surface of each plate, meaning only the wavelengths of standing waves are allowed. This is demonstrated in Fig 1. Although the energies outside and between the plates remain infinite, this results in a finite pressure difference between the two regions, leading to an attractive Casimir Force:

$$F_c(a) = -\frac{\hbar c \pi^2}{240 a^4}. \tag{1.3}$$

If the distance between the plates increases, the number of wave frequencies allowed increases. This reduces the differences between the energies outside and inside the two plates, leading to a reduction in the Casimir Pressure due to $P \propto R^{-3}$ as shown in Eq. (1.4).

$$\frac{\delta E}{L^2} = -\frac{\hbar c \pi^2}{720 a^3}. \tag{1.4}$$

The Casimir effect is influenced by the geometries and material properties of the interacting objects. Spherical symmetries, for instance, can lead to repulsive behaviors, unlike the parallel plate setup. Additionally, the material composition of the interacting objects can also impact the magnitude and behavior of the Casimir force.

Research into the Casimir effect has significantly increased following the successful experiments conducted by Lamoreaux, as mentioned in Section 3.2, and Mohideen (Sec 3.3). The Casimir effect has potential applications in various fields, such as nanotechnology and microelectromechanical systems (MEMS). One possible use-case for the Casimir effect is in the anharmonic oscillator (Sec 4.1).

In summary, the Casimir effect provides an essential link between quantum fluctuations and macroscopic forces, with implications for the understanding of Van der Waals forces and potential applications in various scientific and technological fields. By examining different geometries, material properties, and experimental setups, researchers continue to uncover new insights into this fascinating phenomenon.

2 Mathematical Derivations of Casimir Effect

Regularization techniques are essential in the study of the Casimir Effect because they help address the problem of infinite energy associated with vacuum fluctuations. In quantum field theory, the ground state of an electromagnetic field, also known as the vacuum state, possesses an infinite amount of energy due to continuous oscillations at all frequencies. These infinite energy values pose a significant challenge in understanding and predicting physical phenomena, such as the Casimir Effect. Therefore, regularization techniques are employed to manage these infinities and provide meaningful results that can be applied to real-world scenarios.

2.1 Deriving Using Euler-Maclaurin Formula

One of the widely used regularization techniques is the Euler-Maclaurin formula. The Euler-Maclaurin formula is a powerful mathematical tool that can be applied to approximate the sum of a function over a finite range. By using this formula, we can convert the infinite sum of vacuum energies into a more manageable form. The Euler-Maclaurin formula allows us to obtain finite values for the Casimir force by subtracting the infinite contributions arising from vacuum fluctuations, thereby providing a more accurate understanding of the physical phenomenon.

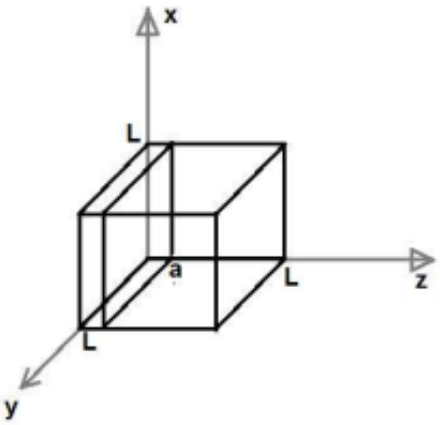

Figure 2: Cubic cavity with dimensions L × L × L surrounded by walls with ideal conduction

Let there be a cubic cavity Fig. 2 with dimensions $L \times L \times L$ surrounded by walls with ideal conduction. The interior of that cavity should be a vacuum. In the plane $z = a$ (so $a << L$) we put another plaque of ideal conductivity.

In a vacuum, angular frequency ω_k is related to the wave number k by the speed of light c :

$$\omega_k = c|\mathbf{k}|, \tag{2.1}$$

Eq. (2.1) allows us to express the zero-point energy of the field as a sum over quantized modes, identified by k_x, k_y and k_z, where:

$$k_x = \frac{n_x \pi}{L}, k_y = \frac{n_y \pi}{L}, k_z = \frac{n_z \pi}{L}, \tag{2.2}$$

The electromagnetic field in the vacuum can be modeled as a quantum harmonic oscillator Eq. (1.2) The harmonic oscillator Hamiltonian is:

$$H = \sum_k \hbar \omega_k \left(n + \frac{1}{2} \right).$$

The average energy of the oscillator in the ground state is:

$$\langle E \rangle = \langle 0 | \hat{H} | 0 \rangle = \left\langle 0 \left| \sum_k \hbar \omega_k \left(n + \frac{1}{2} \right) \right| 0 \right\rangle = \frac{1}{2} \hbar \sum_k \omega_k = \frac{\hbar c}{2} \sum_k \sqrt{k_x^2 + k_y^2 + k_z^2}.$$

Since L is too large, then we may regard k_x, k_y and k_z as continuous variables and $\Delta k_x = \frac{k_x}{n_x} = \frac{\pi}{L} \to 0$, $\Delta k_y = \frac{k_y}{n_y} = \frac{\pi}{L} \to 0, \Delta k_z = \frac{k_z}{n_z} = \frac{\pi}{L} \to 0$ so:

$$\begin{aligned} \langle E \rangle = \\ \approx 2. \frac{\hbar c}{2} \frac{L^3}{\pi^3} \iiint_0^\infty \sqrt{k_x^2 + k_y^2 + k_z^2} dk_x dk_y dk_z. \end{aligned} \tag{2.3}$$

We multiply Eq. (2.3) with 2 due to combined polarizations of the Transverse Electric and Transverse Magnetic fields. The energy throughout the cube is given by:

$$\langle E_L \rangle = 2 \cdot \frac{\hbar c}{2} \frac{L^3}{\pi^3} \iiint_0^\infty \sqrt{k_x^2 + k_y^2 + k_z^2} dk_x dk_y dk_z. \tag{2.4}$$

The energy in the part $z > a$ is (in this case $\frac{k_z}{n_z} = \frac{\pi}{(L-a)}$):

$$\langle E_{L-a} \rangle = 2 \cdot \frac{\hbar c}{2} \frac{L^2 (L-a)}{\pi^3} \iiint_0^\infty \sqrt{k_x^2 + k_y^2 + k_z^2} dk_x dk_y dk_z. \tag{2.5}$$

In the case where $0 < z < a$ since a is too small, we can not consider k_z a continuous variable, so the triple sum returns to a double integral and single sum

$$\langle E_a \rangle = \frac{\hbar c}{2} \frac{L^2}{\pi^2} \sum_{kz} \iint_0^\infty \sqrt{k_x^2 + k_y^2 + k_z^2} dk_x dk_y = \frac{\hbar c}{2} \frac{L^2}{\pi^2} \sum_{(0)1}^\infty \iint_0^\infty \sqrt{k_x^2 + k_y^2 + \frac{n_z^2 \pi^2}{a^2}} dk_x dk_y. \tag{2.6}$$

Where the symbol (0) 1 at the lower limit of the sum means that when $n_z = 0$ the coefficient before the integral is 1 while when $n_z > 0$ then the coefficient before the integral is 2. This is because if $n_z > 0$ we have two present polarizations.

In Eq. (2.6), we move to polar coordinates and replace $n_z = n$ and we get:

$$\langle E_a \rangle = \frac{\hbar c}{2}\frac{L^2}{\pi^2}\sum_{(0)1}^{\infty}\frac{\pi}{2}\int_0^{\infty}\sqrt{r^2+\frac{n^2\pi^2}{a^2}}rdr. \tag{2.7}$$

The difference in the energy of the restricted part and the rest of the cube is:

$$\delta E = E_a + E_{L-a} - E_L. \tag{2.8}$$

After substituting the values in Eq. (2.8) , it becomes:

$$\delta E = \frac{\hbar c}{2}\frac{L^2}{\pi^2}\left\{\sum_{(0)1}^{\infty}\frac{\pi}{2}\int_0^{\infty}\sqrt{r^2+\frac{n^2\pi^2}{a^2}}rdr - \frac{a}{\pi}\int_0^{\infty}\left[\int_0^{\infty}\sqrt{r^2+\frac{n^2\pi^2}{a^2}}rdr\right]dk_z\right\}. \tag{2.9}$$

These integrals are all divergent. However, knowing that high-frequency electromagnetic fields (such as gamma rays, etc.), the waves penetrate the plate without any obstruction(barrier), so functions under integral must be multiplied by a decreasing function of the form:

$$f\left(\frac{k}{k_m}\right) = \begin{cases} 1 \text{ for } k \ll k_m \\ 0 \text{ for } k \gg k_m. \end{cases}$$

And making the substitution: $u = \frac{a^2r^2}{\pi^2}$ in Eq. (2.9). We get:

$$\begin{aligned}\delta E = \frac{L^2\hbar c\pi^2}{4a^3}\Bigg\{&\sum_{(0)1}^{\infty}\left[\int_0^{\infty}\sqrt{u+n^2}f\left(\pi\sqrt{u+n^2}/ak_m\right)du\right] \\ &-\int_0^{\infty}\left[\int_0^{\infty}\sqrt{u+n^2}f\left(\pi\sqrt{u+n^2}/ak_m\right)du\right]dn\Bigg\}.\end{aligned} \tag{2.10}$$

Here we have the difference between a sum and an integral of the same function. In such cases, the Euler-Maclaurin formula is used:

$$\sum_{(0)1}^{\infty}F(n) - \int_0^{\infty}F(n)dn = -\frac{1}{12}F'(0) + \frac{1}{24\cdot 30}F'''(0) + \cdots \tag{2.11}$$

We make the substitution $u+n^2 = w$ and for the function within the sum, respectively the integral, $F(n)$ we have:

$$F(n) = \int_{n^2}^{\infty} w^{1/2} f\left(\frac{w\pi}{ak_m}\right)dw.$$

Using partial integration we get:

$$\begin{aligned} u &= f\left(\frac{w\pi}{ak_m}\right), \quad du = f'\left(\frac{w\pi}{ak_m}\right)\cdot\frac{\pi}{ak_m}dw, \\ dv &= w^{1/2}dw, \quad v = \frac{2}{3}w^{\frac{3}{2}}, \end{aligned}$$

Next, substituting these expressions into the partial integration formula, we get

$$F(n) = \frac{2}{3}w^{\frac{3}{2}} \cdot f\left(\frac{w\pi}{ak_m}\right)\Big|_{w=n^2}^{w=\infty} - \int_{n^2}^{\infty} \frac{2}{3}w^{\frac{3}{2}} f'\left(\frac{w\pi}{ak_m}\right) \cdot \frac{\pi}{ak_m} dw.$$

The function f has been selected such that when $w \to \infty, f \to 0$. Such a function tends to zero faster than it tends to infinity, therefore,

$$\lim_{w\to\infty} \frac{2}{3}w^{\frac{3}{2}} \cdot f\left(\frac{w\pi}{ak_m}\right) = 0.$$

Also, function f tends to zero asymptotic so for large values of w its derivative is practically zero, so for values $w > n^2$ the integral is:

$$\int_{n^2}^{\infty} \frac{2}{3}w^{\frac{3}{2}} f'\left(\frac{w\pi}{ak_m}\right) \cdot \frac{\pi}{ak_m} dw = 0.$$

Therefore,

$$F(n) = -\frac{2}{3}n^3 \cdot f\left(\frac{n^2\pi}{ak_m}\right),$$

For derivatives of this function according to n, we have:

$$F'(n) = -2n^2 f\left(\frac{n^2\pi}{ak_m}\right) - \frac{2}{3}n^3 \cdot f'\left(\frac{n^2\pi}{ak_m}\right) \cdot \frac{\pi}{ak_m} = -2n^2 f\left(\frac{n^2\pi}{ak_m}\right)$$

$$F''(n) = -4nf\left(\frac{n^2\pi}{ak_m}\right)$$

$$F'''(n) = -4$$

$$F'(0) = 0$$

$$F'''(0) = -4.$$

Thus, the difference can be calculated after using Eq. (2.11) in Eq. (2.10):

$$\begin{aligned}\delta E = \frac{L^2\hbar c\pi^2}{4a^3} \Bigg\{ &\sum_{(0)1}^{\infty} \left[\int_0^{\infty} \sqrt{u+n^2} f\left(\pi\sqrt{u+n^2}/ak_m\right) du\right] \\ &- \int_0^{\infty} \left[\int_0^{\infty} \sqrt{u+n^2} f\left(\pi\sqrt{u+n^2}/ak_m\right) du\right] dn \Bigg\} \\ &= \frac{L^2\hbar c\pi^2}{4a^3} \left\{-\frac{1}{12} \cdot 0 + \frac{1}{24\cdot 30} \cdot (-4) + \cdots\right\}\end{aligned}$$

$$\delta E = \frac{L^2\hbar c\pi^2}{4a^3}\left(-\frac{1}{180}\right).$$

The energy (in unit area) becomes:

$$\frac{\delta E}{L^2} = -\frac{\hbar c \pi^2}{720 a^3}.$$

As expected, this matches with the claim made in Eq. (1.4)

$$\frac{F}{L^2} = -\frac{\hbar c \pi^2}{240 a^4} = -0.13 \frac{1}{a^4} \frac{\mu \mathrm{N}}{\mathrm{cm}^2}.$$

This was the mathematical expression of Casimir's force Eq. (1.3), the results of which were confirmed 50 years later.

2.2 Deriving Using Zeta-Function Regularization

Another popular regularization technique is the zeta function regularization. This method relies on the analytical continuation of the Riemann zeta function, which has the unique property of converging to finite values for specific complex numbers. By associating the infinite sums of vacuum energies with the zeta function, we can determine finite values that are physically relevant. The zeta function regularization method is particularly useful in addressing the infinities in quantum field theories, and it has been successfully applied to the study of the Casimir Effect.

With the same physical setup as in Figure 2, the energy between the plates is,

$$\begin{aligned} E &= \frac{\hbar}{2} \sum_k |\omega_k| \\ &= \frac{\hbar c}{2} \sum_k |\mathbf{k}|, \end{aligned}$$

where $\mathbf{k}$ is the wave vector. As $|\mathbf{k}| = \sqrt{k_x^2 + k_y^2 + k_z^2}$,

$$E = \frac{\hbar c}{2} \sum_{k_x, k_y, k_z} \sqrt{k_x^2 + k_y^2 + k_z^2},$$

where k_x, k_y, and k_z are defined in Eq. (2.2). L is infinitely large, so the summation over k_x and k_y becomes an integral from the limits 0 to ∞. Moreover, each quantum fluctuation of wave vector $\mathbf{k}$ has two polarizations. Therefore,

$$\begin{aligned} E &= \frac{\hbar c}{2} \sum_{k_z} \int_0^\infty \int_0^\infty 2\sqrt{k_x^2 + k_y^2 + k_z^2} dn_x dn_y \\ &= \frac{\hbar c L^2}{\pi^2} \sum_{k_z} \int_0^\infty \int_0^\infty \sqrt{k_x^2 + k_y^2 + k_z^2} dk_x dk_y. \end{aligned} \tag{2.12}$$

To solve the double integral, it must be converted to polar coordinates. $dk_x dk_y$ in Eq. (2.12) will be substituted with $\frac{\pi}{2} r dr$, where

$$r^2 \equiv k_x^2 + k_y^2.$$

Therefore,

$$
\begin{aligned}
E &= \frac{\hbar c L^2}{\pi^2} \sum_{k_z} \int_0^{\frac{\pi}{2}} \int_0^{\infty} r\sqrt{r^2 + k_z^2}\, dr d\theta \\
&= \frac{\hbar c L^2}{2\pi} \sum_{k_z} \int_0^{\infty} r\sqrt{r^2 + k_z^2}\, dr.
\end{aligned}
\tag{2.13}
$$

Defining $\omega_n \equiv c\sqrt{r^2 + k_z^2}$ and $|\omega_n|^{-s}$ as a regulator, we substitute these into Eq. (2.13),

$$
\begin{aligned}
E &= \frac{\hbar L^2}{2\pi} \int_0^{\infty} r dr \sum_{n_z=1}^{\infty} \omega_n |\omega_n|^{-s} \\
&= \frac{\hbar L^2}{2\pi} \sum_{n_z=1}^{\infty} \int_0^{\infty} r \left| r^2 + \frac{n_z^2 \pi^2}{a^2} \right|^{\frac{1-s}{2}} c^{1-s} dr.
\end{aligned}
\tag{2.14}
$$

where s can be taken as 0 to satisfy Eq. (2.13).

Using the u-substitution method by defining $u \equiv \left| r^2 + \frac{n_z^2 \pi^2}{a^2} \right|$ and in return getting $du = 2rdr$, we arrive at

$$
\begin{aligned}
E &= \frac{\hbar L^2}{4\pi} c^{1-s} \sum_{n_z=1}^{\infty} \int_{k_z^2}^{\infty} u^{\frac{1-s}{2}} du \\
&= \frac{\hbar L^2}{4\pi} c^{1-s} \sum_{n_z=1}^{\infty} \left(\frac{2}{3-s} \right) u^{\frac{3-s}{2}} \Big|_{k_z^2}^{\infty}.
\end{aligned}
$$

To make the integral convergent and Casimir Energy finite, a condition of $Re(s) > 3$ must be imposed. Thus,

$$
\begin{aligned}
E &= \frac{\hbar L^2}{4\pi} c^{1-s} \sum_{n_z=1}^{\infty} \left[0 - \left(\frac{2}{3-s} \right) \left(\frac{n^{3-s} \pi^{3-s}}{a^{3-s}} \right) \right] \\
&= -\frac{\hbar \pi^{2+s} c^{1-s} L^2}{2(3-s) a^{3-s}} \sum_{n_z=1}^{\infty} \frac{1}{n_z^{s-3}} \\
&= -\frac{\hbar \pi^{2+s} c^{1-s} L^2}{2(3-s) a^{3-s}} \zeta(s-3),
\end{aligned}
\tag{2.15}
$$

where $\zeta(s-3) = \sum_{n_z=1}^{\infty} \frac{1}{n_z^{s-3}}$ is the Riemann-zeta function. For $s = 0$, its solution, using analytic continuation, is

$$
\zeta(-3) = \frac{1}{120}.
$$

By substituting this value into Eq. (2.15), the Casimir Energy per unit area of the plate becomes,

$$
\frac{\delta E}{L^2} = -\frac{\hbar c \pi^2}{720 a^3},
$$

which is the same Eq. (1.4). To calculate the Casimir Force per unit area,

$$\frac{F}{L^2} = \frac{\delta}{\delta a}\left(\frac{E_c}{L^2}\right)$$
$$= -\frac{\hbar c \pi^2}{240 a^4},$$

which is the same expression as in Section 2.1 and Eq. (1.3).

3 The Experimental Proofs of the Casimir Effect

The prediction of the Casimir effect was a significant milestone, as it demonstrated the tangible consequences of vacuum energy and the zero-point energy of quantum fields. However, experimentally verifying it proved to be a challenging task, as sophisticated and precise experimental setups were required to measure the minuscule force between plates and to eliminate various potential sources of error.

3.1 Initial Experiments and the Need for Greater Precision

Spaarnay provided experimental evidence for the Casimir effect in 1958, but the attractive force was not in clear agreement with the prediction given by Eq. (1.4) due to effectively a 100% uncertainty. The exponent in the separation distance 'a' of the original expression had an uncertainty of ± 1 in Spaarnay's experiment, which made it impossible to consider this as proof of the effect. This demonstrated the intricate experimental setup required, and it was not achieved until 1997 by Lamoreaux.

3.2 Lamoreaux's Experiment: Setup, Results, and Consistency with Theory

Steven K. Lamoreaux's experiment in 1997 [3] was instrumental in providing strong experimental evidence for the Casimir effect. In his setup, Lamoreaux used a torsion pendulum in conjunction with a parallel plate configuration. One plate was attached to the pendulum, and the other was mounted on a micrometer-driven translation stage. The plates were made of high-quality, gold-coated mirrors to ensure that they were highly conducting and optically flat. This design allowed for precise control over the plate separation and accurate measurement of the small attractive force between the plates.

The original thought experiment was designed to be conducted in a perfect vacuum with perfectly conducting metals. This was, however, very difficult to achieve. Nevertheless, Lamoreaux was able to reach an appreciable level of accuracy. One aspect of inaccuracies he had to deal with was the electric forces in the setup despite the plates being uncharged. These electric forces were a consequence of voltage differences when two metals used in the setup came into contact. Lamoreaux tried to remove this force by applying an equal and opposite potential across the setup.

Nevertheless, these electric forces were significant in comparison to the Casimir force measured. At a distance of 0.6 μm, the Casimir force was still only a mere 20% percent of the calculated electric force. As the electric force is proportional to $\frac{1}{a}$ and the Casimir force is proportional to $\frac{1}{a^3}$ (a is the separation distance between the plate and the sphere),

the electric force was very significant compared to the Casimir force as distance increased Fig. 3.

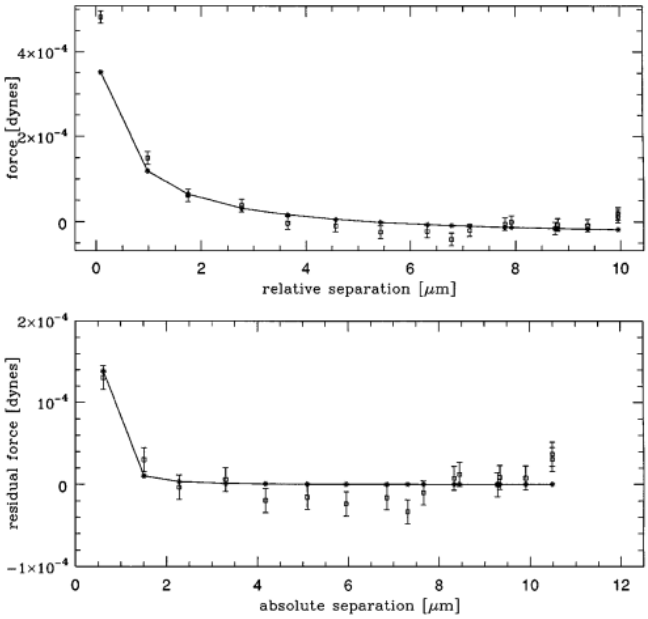

Figure 3: Top: Force measurements based on the relative position and least-squares fitting to $F_c^T(a_i 1 + a_0) + \frac{\beta}{a_i 1 + a_0} + b$; the two closest approach points were excluded from the fit. Bottom: Force measurements with the electric contribution removed; the points connected by lines correspond to the anticipated Casimir force.

To minimize potential sources of error, Lamoreaux carefully considered and addressed several factors, such as surface roughness, residual electrostatic forces, and thermal effects. The surface roughness of the plates was controlled by polishing and cleaning, while electrostatic forces were mitigated by grounding the plates and ensuring low residual potential differences between them. Temperature effects were managed by maintaining a stable laboratory environment and accounting for the thermal expansion of the materials used.

The experimental results demonstrated that the Casimir force between the plates was indeed attractive, as predicted by the theory. The measured force was found to be in good agreement with the theoretical expression in Eq. (1.3) The force was observed to vary with the plate separation, and Lamoreaux reported a 5% uncertainty in the measured force, which was a significant improvement over previous experiments.

However, the setup could not measure values of a less than 0.6 μm, which Lamoreaux suggested could be due to *dirt on the system* or an error in the feedback loop. He also pointed out that the setup was not accurate enough to detail finite temperature changes.

Lamoreaux's experimental results were consistent with the theoretical prediction of the Casimir effect, confirming the presence of an attractive force between uncharged conducting plates in a vacuum. This experiment marked a crucial milestone in the experimental verification of the Casimir effect and paved the way for subsequent advancements in the

field.

3.3 Mohideen's Experiment: Setup, Results, and Consistency with Theory

In 1998 [4], Umar Mohideen and his collaborators conducted another important experiment to further improve the accuracy of Casimir force measurements. Mohideen's experiment employed a different approach, using an atomic force microscope (AFM) with a sphere-plane geometry instead of the parallel plate configuration used by Lamoreaux. This method allowed for increased sensitivity and more precise control over the force measurements.

In Mohideen's experimental setup, a polystyrene sphere coated with gold and having a radius of R was affixed to the atomic force microscope's cantilever. Opposite the sphere, a flat plate, also coated with gold, was positioned. The use of gold coatings ensured high conductivity and compatibility with the theoretical predictions for the Casimir effect. The sphere-plane geometry facilitated a more straightforward calculation of the Casimir force, as the force between the sphere and the plate could be directly measured using the deflection of the cantilever.

The Casimir force F in the sphere-plane geometry can be related to the force between parallel plates using the proximity force approximation (PFA), given by:

$$F_{\text{sp}} \approx 2\pi R F_{\text{pp}},$$

where F_{sp} is the Casimir force between the sphere and the plane, F_{pp} is the Casimir force per unit area between parallel plates, and R is the radius of the sphere. The force per unit area between parallel plates is given by the same expression used in Lamoreaux's experiment and the theoretical prediction given by Casimir in Eq. (1.3).

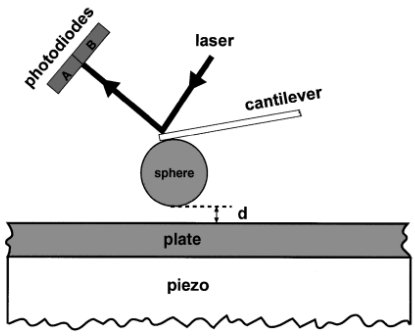

Figure 4: Diagram illustrating Mohideen's experimental configuration. By applying a voltage to the piezoelectric element, the plate moves towards the sphere. Experiments were conducted at a pressure of 50 mTorr and room temperature.

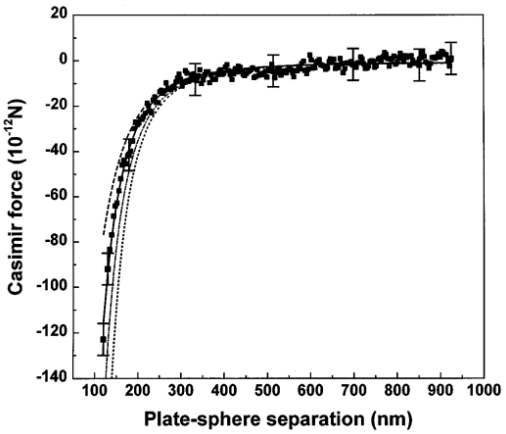

Figure 5: The average Casimir force measured across 26 scans

To minimize sources of error, Mohideen and his team carefully considered factors such as surface roughness, residual electrostatic forces, and temperature effects. The gold coatings

provided smooth surfaces with minimal roughness, while the residual electrostatic forces were mitigated by grounding both the sphere and the plate. Temperature effects were controlled by maintaining a stable laboratory environment and accounting for the thermal expansion of the materials used.

The experimental results from Mohideen's experiment were consistent with the theoretical predictions of the Casimir effect. The measured Casimir force exhibited the expected inverse fourth power dependence on the sphere-plane separation, as described by the proximity force approximation for the sphere-plane geometry. Importantly, Mohideen's experiment achieved an impressive 1% uncertainty in the measured force, further strengthening the experimental verification of the Casimir effect.

Mohideen's experiment, building on the success of Lamoreaux's work, significantly improved the accuracy and reliability of Casimir force measurements, establishing the Casimir effect as an essential aspect of quantum field theory and its real-world consequences.

4 Applications in Nanotechnology

The Casimir Effect can effectively account for or explain multiple aspects of a system at the nanoscale. Since advances in technology are based on greater functionality while reducing device size, it must be dealt with or manipulated within the system so that greater efficiency can be achieved.

In nanomechanical systems (NEMS) or micromechanical systems (MEMS), the separation between moving components and fixed electrodes is minuscule. Therefore, smaller voltages applied must generate larger actuating forces or torques. However, such a feat becomes restricted because of stiction in the device, which is the friction that needs to be overcome for motion. It has been observed that the Casimir Force is responsible for its occurrence. Moreover, radio-frequency transmitters and receivers have a high-quality factor Q for narrow bandwidth operations. However, because of the Casimir Force, some of the mechanical energy is dissipated, leading to a decrease in Q and increased crosstalk with nearby receivers. Thus, it is essential to take the Casimir Effect into account while designing NEMS and MEMS, as otherwise, it would cost its functionality [5].

4.1 Anharmonic Casimir Oscillator

One such device design that has in-build corrections to the Casimir Effect is the Anharmonic Casimir Oscillator (ACO) [6]. It is a MEMS device whose oscillatory motion deviates from that of a simple harmonic oscillator, hence anharmonic. It has two parallel plates, one being movable and the other being fixed, at a separation distance a. The motion of the former resembles that of a linear spring system with spring constant k, indicating some Hooke's law characteristics, as shown in Figure 6.

Therefore, the total potential energy per unit area in the system is the sum of the elastic potential and Casimir energies:

$$U(a) = \frac{k(b-a)^2}{2A} - \eta\frac{\hbar c\pi^2}{720a^3}, \tag{4.1}$$

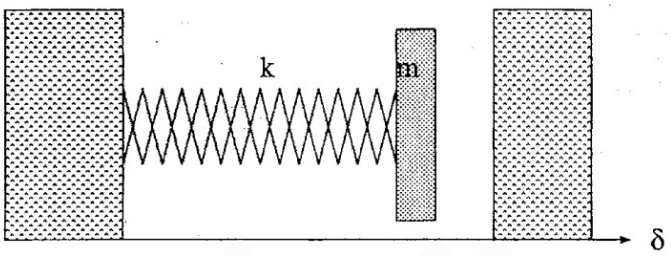

Figure 6: Structure of an Anharmonic Oscillator.

where b is the total separation between the fixed components, A is the area of the plate, and η is the phenomenological prefactor which considers the static electric permittivity of the plate and its value is in between the range of

$$0 < \eta \leq 1.$$

When $\eta = 1$, the plates become perfectly conducting, thus the second term in Eq. (4.1) becomes the Casimir energy derived in Eq. (1.4).

To understand the various energy dynamics at play, some more variables ought to be defined, especially the normalized displacement δ of the moving plate

$$\delta \equiv \frac{\omega}{\omega_0},$$

where ω is the nonnormalized displacement of the movable plate and ω_0 is the nonnormalized displacement of the stationary plate, both from the point where the extension of the spring is 0. Similarly, a positive dimensionless characteristic constant C is defined as

$$C \equiv \frac{\Gamma}{k\omega_0^5},$$

where $\Gamma \equiv \frac{\hbar c \pi^2}{240}$. C can be thought of as a ratio of Casimir force F_C on the movable plate at $\omega = 0$, i.e. no deflection, to the elastic force F_k on the movable plate at $\omega = \omega_0$, i.e. full deflection. At different values of C, the normalized potential energy $\frac{U}{E_k}$ changes with respect to increasing δ, as shown in Figure 7. Here, we observe three ranges of C whose shape of normalized potential energy with respect to δ is distinct from each other.

When $0 < C < C_{cr}$, where C_{cr} is the critical value of C beyond which the movable plate simply collapses into the stationary plate on the right, the normalized potential energy has a minimum potential energy U_{min} at δ_{min} and a maximum potential energy U_{max} at δ_{max}. The local minima and maxima for U_{min} and U_{max} respectively for the aforementioned range can be seen in Figure 8. This is the "separation state" of the ACO, where the movable plate oscillates about a stable equilibrium state (at δ_{min}), while not having enough kinetic energy to move past an unstable equilibrium state (at δ_{max}).

When C approaches C_{cr}, the shape of the normalized potential changes to a point where, instead of local minima or maxima, both δ_{min} and δ_{max} converge to form an inflection point, as seen in Figure 7 and Figure 8.

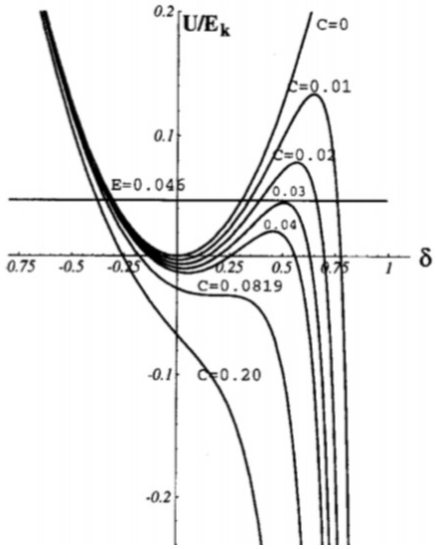

Figure 7: Changes in the normalized potential energy $\frac{U}{E_k}$ with respect to δ for particular values of C. $C = 0.0819$ is the critical value known as C_{cr}, which produces an inflection point in its graph. From $0 < C < C_{cr}$, there is a local minima and local maxima at δ_{min} and δ_{max} respectively. From $C > C_{cr}$, there is no inflection point.

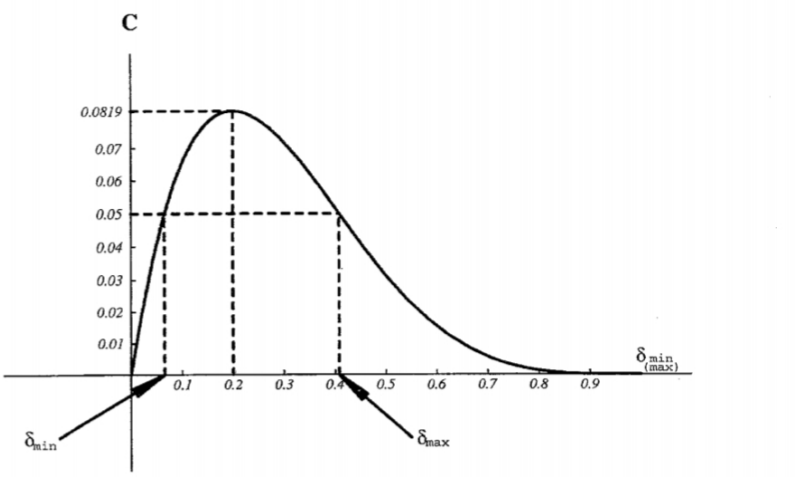

Figure 8: The corresponding values of δ_{min} and δ_{max} of $C < C_{cr}$. As C approaches $C_{cr} = 0.0819$, a maximum is reached, indicating that $\delta = \delta_{min} = \delta_{max} = 0.2$.

When $C > C_{cr}$, as k decreases, the movable plate comes in contact with the stationary plate. This is the "contact state" of the ACO. Under ideal conditions, where the plates have smooth surfaces, the normalized potential energy is negative infinity, as shown in Figure 7. However, realistically, there is always some non-zero normalized minimum gap ζ in between the minute rough edges of the plates, and so the contact state occurs when $\delta = 1 - \zeta$. Generally, it is not desirable to be in this state because it may lead to increased stiction, and restoring separation between the two plates may be tedious.

The ACO can oscillate anharmonically between two of its stable equilibrium states: the separation state, and the contact state. By manipulating these system dynamics and their sensitivity to changes in C, it can be used in multiple sensors and detectors. As the sizes of MEMS are becoming more and more minuscule, this ACO modeling displays the importance of incorporating the influences of the Casimir Effect into its mechanics so as to increase its operational performance and avoid system inefficiencies.

4.2 Hurdles in Applications

The implementation of Casimir forces in future nanotechnological applications faces several challenges, primarily due to the inherent complexities associated with the size, material, and geometry of the components involved. These hurdles must be overcome for the successful integration of Casimir forces in next-generation devices and systems.

One major challenge in harnessing Casimir forces for nanotechnology is the diverse range of geometries that may be encountered. For instance, spherical shells generate repulsive Casimir forces, whereas parallel plates yield attractive forces. As a result, devices containing different geometrical configurations would necessitate distinct approaches to effectively manipulate such forces at play.

Another obstacle is their sensitivity to background noise, specifically thermal radiation. At elevated temperatures, Casimir forces generally increase due to enhanced thermal fluctuations. Consequently, designing devices that account for these variations in force becomes crucial to ensure optimal performance. In some cases, maintaining a specific operating temperature might be necessary to achieve consistent functionality.

Moreover, material choice for plates plays a significant role in the behavior of Casimir forces. Different materials exhibit distinct properties, which can considerably influence the magnitude and characteristics of the Casimir forces experienced. In the case of ACO in Section 4.1, η depends on material properties, and so the amount of energy dissipated would differ for dissimilar materials. Therefore, their careful selection and an in-depth understanding of their impact on the system are essential for the successful implementation of Casimir forces in nanotechnological applications.

Overcoming the challenges related to geometry, background noise, and material choice is critical for the practical utilization of Casimir forces in future nanotechnology. As research progresses, it is expected that novel solutions and techniques will emerge to address these issues, paving the way for innovative applications and devices that harness the unique properties of Casimir forces.

5 Conclusion

In short, the Casimir Effect is a phenomenon that arises from the behavior of electrodynamic oscillators in ground states, both in a vacuum and between parallel plates. The existence of attractive forces between these plates, proportional to a^{-4}, is a key aspect of the Effect, which has been experimentally validated multiple times.

At the time when Casimir predicted these forces, not much attention was paid to them. However, in recent decades, extensive research has been done on the Casimir Effect as it emphasizes the importance of quantum electrodynamics over classical electrodynamics because the latter would not have predicted it. Moreover, we further examined how geometrical configurations influence the value and sign of the Casimir forces, like in the case of spherical configurations which result in repulsive forces rather than attractive ones.

Although Casimir's initial suggestion - that his eponymous force stabilizes electrons as spheres with a specific radius - has been dismissed, the Casimir force plays a significant role in nanotechnological devices and in its further future nanotechnological development. While the exact nature of this role is complex and not fully understood, ongoing research is expected to reveal more about the potential applications and implications of the Casimir Effect, leading to groundbreaking advancements in various fields.

References

[1] Hendrik Casimir. On the attraction between two perfectly conducting plates. *Proceedings of the Royal Netherlands Academy of Arts and Sciences*, 51:793–795, 1947.

[2] Hendrik Casimir. Some remarks on the history of the so-called casimir effect. *Physics Today*, 52(11):29–31, 1998.

[3] Steve K Lamoreaux. Demonstration of the casimir force in the 0.6 to 6 μm range. *Physical Review Letters*, 78(1):5–8, 1997.

[4] Umar Mohideen and Anushree Roy. Precision measurement of the casimir force from 0.1 to 0.9 μm. *Physical Review Letters*, 81(21):4549–4552, 1998.

[5] M. Bordag, G.L. Klimchitskaya, Umar Mohideen, and V.M. Mostepanenko. *Advances in the Casimir Effect*. Oxford University Press Inc., 2009.

[6] F. Micheal Serry, Dirk Walliser, and G. Jordan Maclay. The anharmonic casimir oscillator (aco) - the casimir effect in a model microelectromechanical system. *Journal of Micromechanical Systems*, 4(4):193–205, 1995.